Gold anode corrosion in an aqueous solution of 2,2-dimethyl-1,3-diaminopropane

M. D. Vedenyapina, V. V. Kuznetzov, A S. Dmitrenok, M. E. Minyaev, N. N. Makhova, and M. M. Kazakova*

N. D. Zelinsky Institute of Organic Chemistry, Russian Academy of Sciences, 47 Leninsky prosp., 119991 Moscow, Russian Federation. E-mail: mvedenyapina@yandex.ru

The kinetics and mechanism of corrosion of an Au anode in a weakly basic aqueous solution of 2,2-dimethyl-1,3-diaminopropane (2,2-DM-1,3-DAP) were studied by gravimetry and cyclic voltammetry. Scanning and transmission electron microscopy was used to determine that under galvanostatic conditions the products of anode corrosion are reduced on a steel cathode with the formation of not only an electrolytic Au deposition on the cathode, but also colloidal gold nanoparticles in the electrolyte medium. The product of the interaction of 2,2-DM-1,3-DAP with atmospheric CO_2, namely, the carbamic acid internal salt 3-ammonio-2,2-dimethylpropylcarbamate, was isolated from the reaction solution.

Key words: 2,2-dimethyl-1,3-diaminopropane, Au electrode, kinetics, corrosion, colloidal gold nanoparticles, carbamic acid, internal salt.

Metallic gold is characterized by resistance to chemical and electrochemical action. It is extracted from mineral raw materials using potassium cyanide solutions. The search for safer methods of extracting gold from minerals, including electrochemical methods, has been carried out over many years.[1—3] It was shown that the anodic dissolution of a gold electrode can take place both in $HClO_4$ or H_2SO_4 solutions containing chloride or bromide ions,[4—6] and in solutions of various organic compounds capable of complexation. For example, in the work,[7] the authors suggested that in solutions of 3-mercaptopropionic and *meso*-2,3-dimethylsuccinic acids in the presence of $LiClO_4$ gold forms coordination compounds with these ligands. Our earlier studies showed that anodic corrosion of an Au electrode effectively proceeds in weakly basic aqueous solutions (0.05 *M* K_2CO_3 solution) of a series of organic bases: hexahydropyrimidine (**1**),[8] 1,5-diazabicyclo[3.1.0]-hexane (**2**),[8,9] 6-methyl-1,5-diazabicyclo[3.1.0]hexane (**3**),[8,9] 6,6-dimethyl-1,5-diazabicyclo[3.1.0]hexane (**4**),[8,9] 1,3-diaminopropane (1,3-DAP) (**5**),[10,11] ethylenediamine (**6**),[11,12] 1,4-diaminobutane (1,4-DAB) (**7**),[11,13] and 1,2-diaminopropane (**8**).[14]

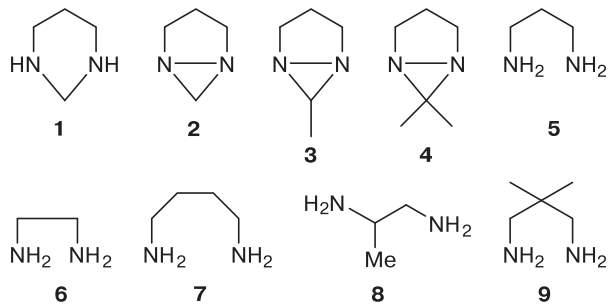

The corrosion of an Au electrode in solutions of organic bases **1**—**8** and the transfer of gold to the cathode with the formation of a compact precipitate were studied in the works[8—14] by gravimetry. The mass of gold contained in the solution during any moment of electrolysis can be determined by calculations based on gravimetry results (the difference in anode and cathode mass). In a number of cases, the products formed during gold corrosion, specifically, Au complexes with the corresponding ligands, were isolated.

In the work,[11] diaminoalkanes **5**—**8** were studied by cyclic voltammetry (CV) for a more detailed investigation of the mechanism of gold corrosion in diamine solutions. A comparative analysis of the cyclic voltammograms registered for gold electrodes in solutions of the investigated compounds showed that only 1,2-diaminoalkanes **6** and **8** are strongly adsorbed on the gold anode surface, completely blocking it, while diaminoalkanes **5** and **7** do not exhibit such strong adsorption. As a result, a linear dependence of anodic peak currents on potential scanning rate was observed only for diaminoalkanes 1,3-DAP and 1,4-DAB.

In this work, we use CV and gravimetry to investigate the kinetics and mechanism of gold corrosion in a solution of previously unexplored 2,2-dimethyl-1,3-diaminopropane (2,2-DM-1,3-DAP) (**9**). It was expected that this diaminoalkane would have a greater tendency to form coordination bonds with gold compared to 1,3-DAP due to the $+I$-effect of the two methyl substituents in the

Published in Russian in *Izvestiya Akademii Nauk. Seriya Khimicheskaya,* No. 4, pp. 735—744, April, 2021.

aliphatic part of the molecule and the limitation of the conformational mobility of the chain.

Experimental

We used commercially available 2,2-dimethyl-1,3-diaminopropane **9** (ACROS). Working solutions were prepared in bidistilled water. Analytical grade potassium carbonate K_2CO_3 was used. Cyclic voltammograms were obtained using a computer-controlled IPC-Compact potentiostat in a three-electrode cell. An Au wire (99.99% Au), sealed into glass, 0.3 mm in diameter and 0.3 cm in length was used as a working electrode; a steel wire with the same dimensions and sealed into glass acted as an auxiliary electrode; a silver chloride electrode (Ag/AgCl/3*M* KCl) served as a reference electrode. The supporting electrolyte was 0.05 *M* K_2CO_3 solution (pH 11.1). The concentration of 2,2-DM-1,3-DAP was 0.1 mol L^{-1}. During study by CV, the potential scanning rate was varied ν, mV s^{-1}: 200, 175, 150, 125, 100, 75, 50, 25.

Anodic corrosion of gold was carried out in a two-electrode cell without separate anode and cathode compartments. Gold and steel wires 0.3 mm in diameter, immersed in an electrolyte solution by 15 mm, served as the anode and the cathode, respectively. Electrolysis was carried out in the galvanostatic mode at 25 °C. The volume of the working solution was 20 mL.

The process was characterized by a decrease of electrode mass. The electrodes were weighed on an ABJ220-4NM electronic analytical balance (Kern, United States) (d = 0.0001 g) at specific time intervals for 50 h.

To isolate product **10**, obtained after electrolysis of the Au anode in a solution of diamine **9**, the reaction solution (electrolyte) was placed in a vacuum desiccator over NaOH for drying at room temperature until the water was completely evaporated after 2—3 days. The resulting solid residue was extracted with methanol (2×50 mL), followed by concentration of the solvent *in vacuo*.

The structure of the obtained new compound **10** was determined by IR and NMR spectroscopy. IR spectra were recorded on a Bruker Alpha instrument in the range 400—4000 cm^{-1}. The IR spectrum of the starting diamine **9** was recorded using a thin layer between KBr plates, while that of the new compound **10** was obtained by pressing the sample with KBr.

For the starting compound **9**, ^1H and ^{13}C NMR spectra were recorded on a Bruker AM-300 spectrometer (operating frequency 300 MHz for ^1H and 75.47 MHz for ^{13}C); for the new compound **10**, 1D and 2D ^1H and ^{13}C NMR spectra were recorded on a Bruker AV-600 spectrometer (600 and 150.90 MHz, respectively). The position of the signals in the ^1H NMR spectra was determined relative to the signals of the residual protons of the deuterated solvent (D_2O). The ^{13}C NMR spectra were recorded relative to tetramethylsilyl propionate (TSP), a chemical shift standard. All correlation NMR spectra were obtained using standard Bruker software. Acquisition time of NOESY was 0.7 s.

The microstructure of the electrodes obtained after the electrolysis of gold in an aqueous solution of diaminoalkane **9** was studied by field emission scanning electron microscopy (FE-SEM) using a Hitachi SU8000 electron microscope. The images were taken in the secondary electrons registration mode at an accelerating voltage of 2—30 kV and a working distance of 8.4—11.0 mm. The study of the samples by energy-dispersive X-ray spectroscopy (EDX) was carried out using an OxfordInstruments X-max energy-dispersive spectrometer (United Kingdom). After electrolysis in a diaminoalkane **9** solution, gold and steel wire samples were placed on the surface of an aluminum table with a diameter of 25 mm and were fixed with two screws. Elemental analysis of samples of products obtained after electrolysis was carried out on a PerkinElmer model 2400 CHN analyzer.

The morphology of colloidal gold particles obtained after electrolysis of the gold anode in an aqueous solution of diaminoalkane **9** was investigated by transmission electron microscopy (TEM) on a Hitachi HT7700 electron microscope (Japan). The images were taken in the transmitted electrons registration mode (bright field mode) at an accelerating voltage of 100 kV. The working solution was applied to a thin carbon film fixed on a copper mesh with a diameter of 3 mm. The mesh was then fixed in a special holder. The sample was applied in liquid form, followed by vacuum drying. The optimization of analytical measurements was carried out within the framework of the previously described approach.[15]

2,2-Dimethyl-1,3-diaminopropane (9) (2,2-DM-1,3-DAP). IR, ν/cm^{-1}: 518, 559, 721 (ρ(CH_2)), 843, 918 (ω(NH_2)), 1065, 1144, 1208, 1235, 1316, 1367 (δ(CH_3)), 1389, 1472 (δ(CH_2)), 1602 (δ(NH_2)), 2206, 2864 (ν_s(CH_2)), 2909, 2951 (ν_s(CH_3)), 3299 (ν_s(NH_2)), 3374 (ν_s(NH_2)). ^1H NMR (D_2O), δ: 0.92 (s, 6 H, Me); 2.49 (s, 4 H, CH_2). ^{13}C NMR (D_2O, TSP), δ: 23.4 (Me), 36.4 (C), 50.3 (CH_2).

3-Ammonio-2,2-dimethylpropylcarbamate (10). IR, ν/cm^{-1}: 540, 620, 702 (ρ(CH_2)), 814, 886, 917, 1020, 1090, 1143

Table 1. Basic crystallographic data and structure refinement statistics for compound **10**

Parameter	**10**
Molecular formula	$C_6H_{14}N_2O_2$
Molecular weight/g mol^{-1}	146.19
Crystal system	Orthorhombic
Space group	$P2_12_12_1$
a/Å	5.7450(1)
b/Å	10.0815(2)
c/Å	12.9215(3)
V/Å^3	748.39(3)
Z	4
D_{calc}/g cm^{-3}	1.297
μ/mm^{-1}	0.097
θ-Range for data collection/deg	2.56—33.73
Number of reflections	
collected	22938
unique (R_{int})	2981 (0.0604)
with $I \geqslant 2\sigma(I)$	2415
Number of refined parameters	147
R_1 ($I \geqslant 2\sigma(I)$)	0.0418
wR_2 (for all reflections)	0.0981
GOOF on F^2	1.040
Flack parameter	−0.4(6)
Residual electron density ($\Delta\rho_{min}/\Delta\rho_{max}$)/e Å^{-3}	−0.372/−0.254

(ω(NH_2)), 1201, 1231, 1279, 1315, 1376 (δ(CH_3)), 1435, 1483 (δ(CH_2)), 1567 (δ(NH_2)), 1635, 2197, 2375, 2457, 2658, 2787, 2883 (ν_s(CH_2)), 2969 (ν_s(CH_3)), 3390 (ν_s(NH_2)), 3431 (ν_s(NH_2)). ^{1}H NMR (D_2O), δ: 0.82 (s, 6 H, Me); 2.62 (s, 2 H CH_2); 2.80 (s, 2 H CH_2). ^{13}C NMR (D_2O, TSP), δ: 23.6 (Me), 35.4 (C), 47.3 (CH_2), 48.8 (CH_2), 166.0 (CO_2).

A single crystal sample of **10** was obtained by recrystallization from ethanol. X-ray diffraction of crystal **10** was carried out on a Bruker Quest D8 diffractometer equipped with a Photon-III detector (graphite monochromator, φ- and ω-scan techniques, step 0.5°, exposure time 50 s) using X-ray radiation MoKα (λ = 0.71073 Å) at a temperature of 100 K. The data on reflection intensities were obtained using SAINT software.[16] Correction for absorption was carried out semi-empirically on equivalent reflections using SADABS software.[17] The structures were solved by the direct method using SHELXT[18] software and refined by the least squares method in the anisotropic (isotropic for hydrogen atoms) full-matrix approximation on F^2 using SHELXL-2018 software.[19] The positions of all the hydrogen atoms were determined from the electron density difference map. The crystallographic results and X-ray diffraction parameters are given in Table 1. The structural data for compound **10** were deposited with the Cambridge Crystallographic Data Center (CCDC 2039098).

Results and Discussion

Cyclic voltammetry resulted for a gold electrode in a solution of the studied diaminoalkane **9** in the range of potentials from −200 to +1200 mV and for different scanning rates (Fig. 1) show that responses on the anodic and cathodic branches can be observed in the first and subsequent cycles. This indicates the absence of strong adsorption of the ligand, leading to passivation of the anode surface. The anodic branches have peaks in the range of potentials E = 400—1000 mV. The $I_{p,a}$ values increase with the potential scanning rate (v). The potentials at these current maxima are 200 mV higher than the potentials on the cyclic voltammograms recorded for gold in a solution of compound **5** with a potential scanning rate of 200 mV s^{-1} (see the results in Refs 10 and 11).

Due to the high potential of the current maximum on the anodic branch of the cyclic voltammogram, the stoichiometry of the anodic process could not be determined directly. Apparently, the anodic process is multielectron, and each anodic peak is the sum of peaks corresponding to the transfer of individual electrons. This is indirectly confirmed by the absence of a linear dependence of the current maxima on the potential scanning rate for the anodic process.

In the reverse scan of potential, the cathodic branches are shown to have peaks in the range of potentials E = 300—0 mV, the presence of which indicates the reduction of the products of corrosion of the Au anode. The currents corresponding to the maxima of the cathodic peaks ($I_{p,c}$) depend linearly on the potential scanning rate (Fig. 2). This indicates that the reduction of the products of the gold corrosion process proceeds directly on the electrode surface, and the rate-limiting step of the reaction is electron transfer. In this case, the Laviron equation applies:[20]

$$I_{p,c} = nFQv/4RT,$$

where n is the number of electrons participating in the reaction calculated per molecule, F is the Faraday constant equal to 96485 C mol^{-1}, Q is the charge corresponding to the area of the peak on the cathodic branch, v is the potential scanning rate, mV s^{-1}, R is the gas con-

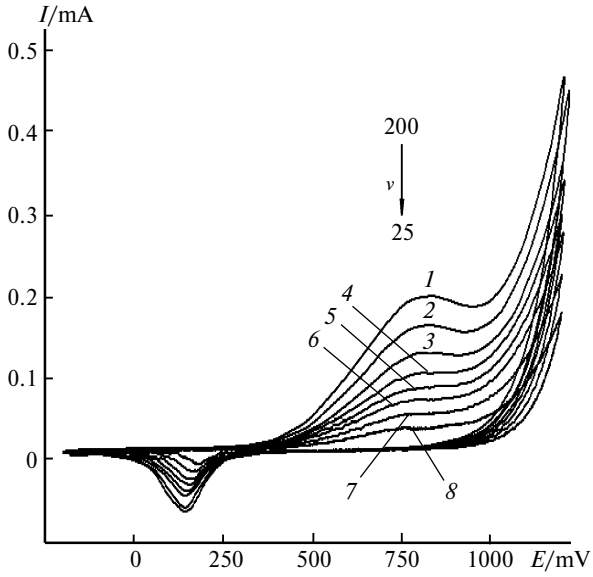

Fig. 1. Cyclic voltammograms of a solution of diaminoalkane **9** taken at different potential scanning rates, v(mV s^{-1}): 200 (*1*), 175 (*2*), 150 (*3*), 125 (*4*), 100 (*5*), 75 (*6*), 50 (*7*), and 25 mV s^{-1} (*8*).

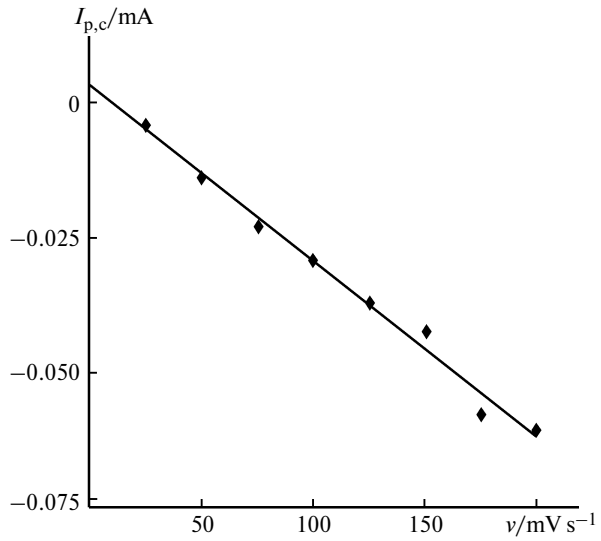

Fig. 2. Dependence of cathodic current maxima on the potential scanning rate (according to CV).

stant equal to 8.314 J mol^{-1} K^{-1}, T is the absolute temperature, K.

The number of electrons participating in the reaction was calculated for the cathodic process using the Laviron equation. The value of n was equal to 2.05—1.84 in the range v = 200—120 mV s^{-1}. Therefore, two electrons participate in the process of cathodic reduction of corrosion products in the diaminoalkane **9** solution.

According to the results of the work,[11] there is a decrease in $I_{p,c}$ and $I_{p,a}$ and an increase in $E_{p,a}$ in the series of diamines **6**, **8**, **5**, **7**. This indicates that the corrosion of the Au anode proceeds more easily in the substrate **6** solution. The investigated diamine **9** exhibits the least activity in the gold corrosion process in comparison with the previously[11] studied substrates.

This regularity in the change of the electrochemical properties of the Au anode in various diamines can be related both to the difference in electron density on nitrogen atoms in these compounds and to the action of structural factors.

Similarly to the works,[8—10,12—14] it was shown by gravimetry method that the Au anode undergoes corrosion with a loss of mass during electrolysis in a solution of diaminoalkane **9** (I = 10 mA). During this process, metallic gold is deposited on the cathode (steel wire). Figure 3 shows the kinetics of the decrease of mass of the gold anode (m_{corr}) and the increase of mass of the cathode deposition (m_{dep}). The difference between these values was used to calculate the mass of gold in the working solution (m_{sol}). It was shown that m_{corr} increases linearly during electrolysis, while m_{dep} and m_{sol} increase nonlinearly, but monotonically. When comparing the obtained results with those of the works,[10,12] where other diaminoalkanes were used as ligands, some similarities can be observed, however, for the same duration of electrolysis, the mass of corroded gold in diamine **9** solution is less than in solutions of compounds **5**—**8** (Table 2).

Similarly to previously published works,[8—10,12—14] when interpreting the observed kinetic regularities, the sum of the reactions of anodic dissolution and cathodic precipitate of gold can be represented in the form of a system of differential equations:

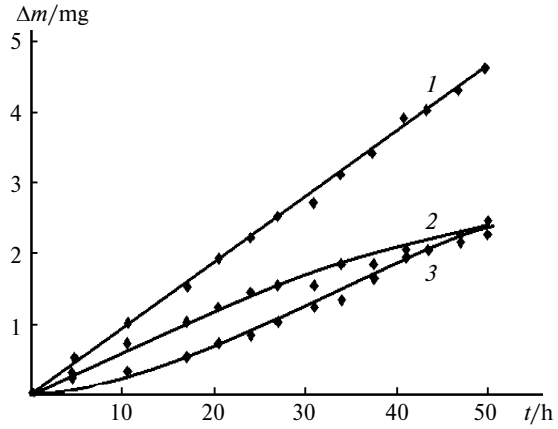

Fig. 3. Kinetics of decreasing Au anode mass (m_{corr}, *1*) and increasing cathodic deposition mass (m_{dep}, *2*) and gold mass in the solution (*3*).

$$dm_1/dt = k_1, \quad (1)$$

$$dm_2/dt = k_1 - k_2 m_2, \quad (2)$$

$$dm_3/dt = k_2 m_2, \quad (3)$$

where m_1 is m_{corr}, m_2 is m_{sol}, and m_3 is m_{dep}. The solution of this system of equations using the Mathcad system made it possible to find k_1 and k_2 for diaminoalkane **9**, which most accurately describe the experimental results shown in Fig. 3. The values k_1 and k_2 are given in Table 2 and are equal to 0.09 mg h^{-1} and 0.02 h^{-1}, respectively, for substrate **9**. Comparing the constants k_1 and k_2 for the substrates given in Table 2, it can be inferred that different the corrosion process in the diamine **9** solution studied in this work is more difficult and slower. This is also confirmed by the rate of dissolution of the gold anode during electrolysis given in Table 2. The intensity of the electrochemical process occurring at the cathode with the participation of the studied substrate **9**, taking into account the constant k_2, is also the lowest compared to all the previously studied substrates (see Table 2).

After the completion of electrolysis of a diamine **9** solution using an Au anode, the anode, the cathode, and

Table 2. Kinetic and electrochemical characteristics of gold corrosion in aqueous solutions of diaminoalkanes

Compound	k_1/mg h^{-1}	k_2/h^{-1}	*E_a/mV	Dissolution rate /mg cm^{-2} h^{-1}	Reference
1,2-Diaminopropane **8**	0.31	0.060	600	4.76	11, 14
1,3-Diaminopropane **5**	0.42	0.040	680	6.66	10, 11
Ethylenediamine **6**	0.55	0.110	572	8.73	11, 12
1,4-Diaminobutane **7**	0.23	0.035	660	3.65	11, 13
2,2-Dimethyl-1,3-diaminopropane **9**	0.09	0.020	770	1.43	Present work

*E_a is the potential of the current maxima on the anodic branch of the cyclic voltammogram.

the electrolysis products were studied before and after extraction. During the corrosion of gold in a substrate **9** solution with a current of 10 mA, a deposition of gold is formed on the cathode, and the solution acquires an intense yellow color. Electron microscopy studies demonstrate that during electrolysis the Au anode undergoes corrosion (Fig. 4, *a*), and a deposition of gold in the form of dendrites forms on the surface of the steel cathode (Fig. 4, *b*). The study of the chemical composition of the steel cathode surface by EDX determined the presence of Au on the surface.

When studying the working solution by transmission electron microscopy (TEM), the obtained micrographs (Fig. 5) show colloidal gold particles having a round shape with sizes of 10—30 nm. The review[21] shows TEM images of colloidal gold nanoparticles synthesized by various

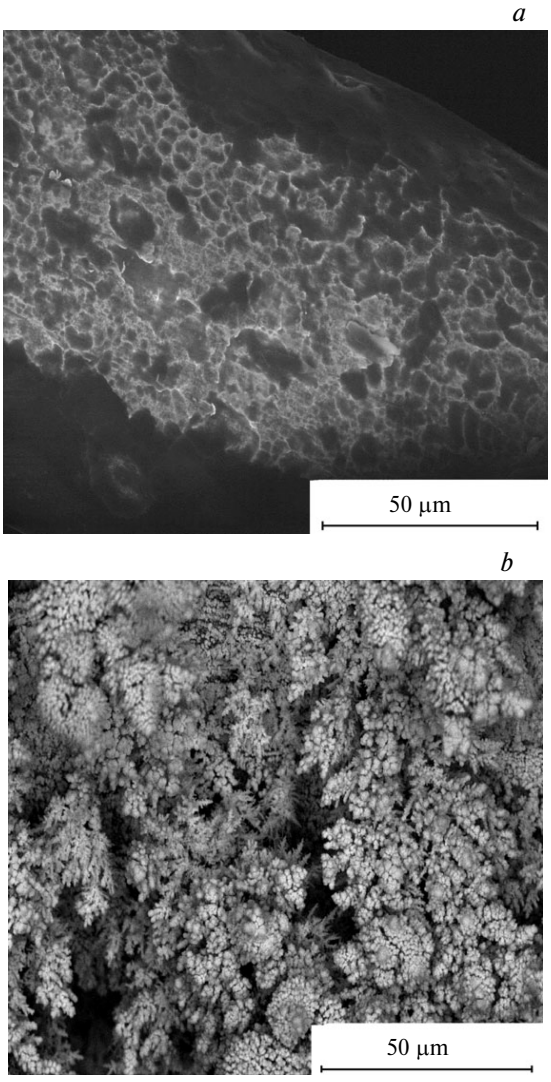

Fig. 4. SEM image of the surface of the Au anode (*a*) and steel cathode (*b*) after electrolysis in an aqueous solution of diaminoalkane **9**.

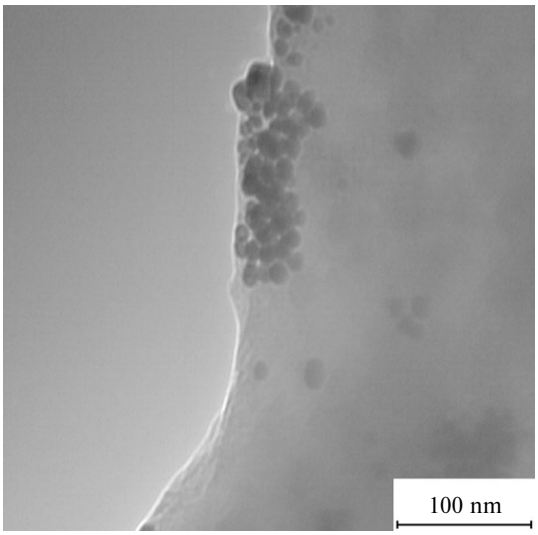

Fig. 5. TEM image of the substrate **9** solution after the anodic dissolution of gold.

chemical methods. Despite the possibility of obtaining colloidal gold by different chemical methods,[20,21] electrochemical synthesis of nanoparticles in diamine solution has been described only in a single work.[14] When extracting the products of electrolysis from the working solution with methanol, colloidal gold particles were not detected by TEM. A solid residue of new compound **10** was obtained after concentrating the methanol extract.

According to IR and NMR spectroscopy, as well as elemental analysis results, it can be assumed that, in contrast to the results presented in the works,[8—10,12—14] the new compound **10** is not a gold complex, because no inorganic residue was found in it. Elemental analysis of the isolated product **10** showed the following ratio of elements (%): C, 49.10; H, 9.81; N, 19.63. If we assume that the composition of the new compound includes oxygen, then with the ratio of elements (%): C, 49.30; H, 9.64; N, 19.16, the molecular formula would be C_3H_7NO or $C_6H_{14}N_2O_2$.

The IR spectra of the starting diaminoalkane **9** and the new compound **10** are shown in Fig. 6.

The spectrum of product **10** shows a shift of the bands corresponding to the stretching and bending vibrations of NH_2, CH_2, and CH_3 groups and contains new bands, which were attributed to the vibrations of the CO group. Thus, the region of stretching vibrations of NH_2 groups reveals a high-frequency shift of the bands of symmetric stretching vibrations $\nu_s(NH_2)$ from 3374 cm^{-1} and 3299 cm^{-1} in the starting diaminoalkane **9** to 3431 cm^{-1} and 3390 cm^{-1} in compound **10** with $\Delta\nu_s = 57$ and 91 cm^{-1}. A high-frequency shift of the band of bending wagging vibrations of the NH_2 group from 918 cm^{-1} to $\omega(NH_2) =$ $= 1143$ cm^{-1} with $\Delta\omega = 225$ cm^{-1} and a low-frequency shift of the band of bending scissoring vibrations from 1602 cm^{-1} to $\delta(NH_2) = 1567$ cm^{-1} with $\Delta\delta = -35$ cm^{-1}

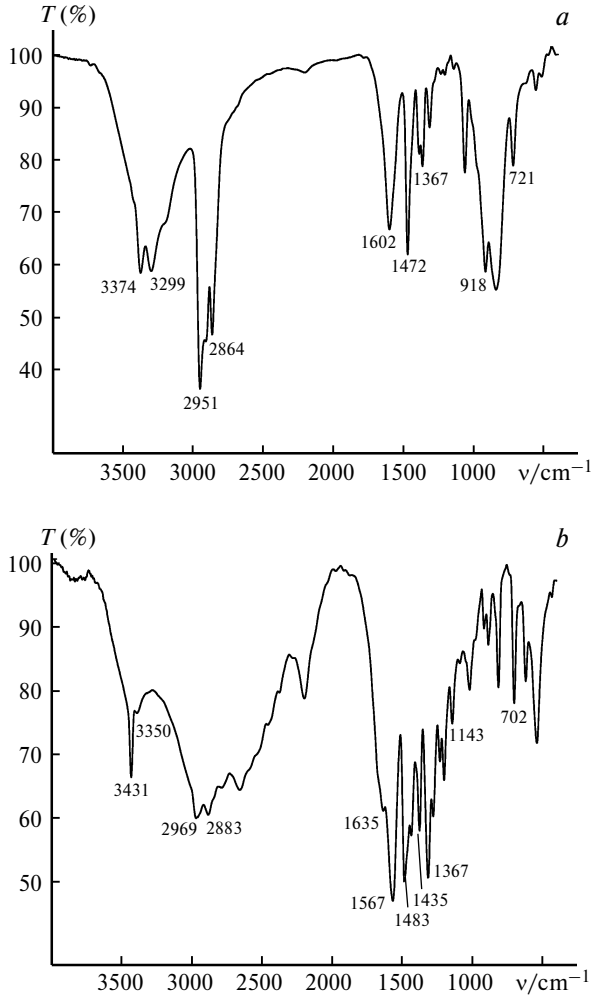

Fig. 6. IR spectra of diaminoalkane **9** (*a*) and new compound **10** (*b*).

is recorded in the spectra of free diamine **9** and product **10**, respectively. In the region of vibrations of the CH_2 group, there is a high-frequency shift of the bending scissoring vibration bands from 1472 cm^{-1} in free 2,2-DM-1,3-DAP **9** to $\delta(CH_2)$ = 1483 cm^{-1} in product **10** with $\Delta\delta$ = 11 cm^{-1} and a low-frequency shift of the bending rocking vibration bands from 721 cm^{-1} in free diaminoalkane **9** to $\rho(CH_2)$ = 702 cm^{-1} in compound **10** with $\Delta\rho = -19$ cm^{-1}. In the region of the main band of symmetric stretching vibrations $\nu_s(CH_2)$, there is also a high-frequency shift from 2864 cm^{-1} in the starting diamine **9** to 2883 cm^{-1} in compound **10** with $\Delta\nu_s$ = 19 cm^{-1}. In the region of stretching vibrations of methyl groups of product **10**, a slight shift of the main band of symmetric stretching vibrations $\nu_s(CH_3)$ = 2969 cm^{-1} ($\Delta\nu_s$ = 18 cm^{-1}) can be observed compared to the starting diaminoalkane **9** (2951 cm^{-1}), and there is also a small high-frequency shift of the main band of bending scissoring vibrations $\delta(CH_3)$ = 1367 cm^{-1} in free 2,2-DM-1,3-DAP to 1376 cm^{-1} in compound **10** with $\Delta\delta$ = 9 cm^{-1}.

The IR spectrum of compound **10** revealed absorption bands ν_{as} = 1567 cm^{-1} and ν_s = 1435 cm^{-1}, which can be attributed to vibrations of the carboxylate anion, bands corresponding to the absorption of the associated amide group $\nu(CO)$ = 1635 cm^{-1} and $\nu(NH_2)$ = 3390 cm^{-1}, as well as an absorption band at 2969 cm^{-1} assigned to the symmetric vibrations of the $\nu_s(NH_3)^+$ group.[23,24] The absorption band at 1567 cm^{-1} is very strong and broad. It probably includes two bands, namely, ν_{as} of the carboxylate anion and ν_{as} of the NH_2 group. Most likely, a similar superposition of absorption bands in the IR spectrum of product **10** is observed for symmetric stretching vibrations $\nu_s(CH_3)$ and $\nu_s(NH_3)^+$ in the region of 2969 cm^{-1}.

In the ^1H NMR spectrum of the starting substrate **9**, the signals of the CH_3 and CH_2 protons appear as singlets with δ = 0.92 and 2.49, respectively (Fig. 7, *a*). In the ^1H NMR spectrum of compound **10**, the signals of the methyl group protons are upfield shifted by $\Delta\delta$ = 0.1 ppm and are registered as singlet with δ = 0.82. The signals of the CH_2 group proton belonging to compound **10** are chemically nonequivalent and are registered as two singlets with δ = 2.62 and 2.80 with a downfield shift of $\Delta\delta$ = 0.13 and 0.31 ppm relative to the starting substrate **9** (Fig. 7, *b*).

In the ^{13}C NMR spectrum of new compound **10**, the carbon atoms of the CH_2 groups are registered as two signals with δ = 47.3 and 48.8, in contrast to the single signal observed for the starting diaminoalkane **9** (Fig. 7, *c*). Both signals are upfield shifted ($\Delta\delta$) relative to the analogous signal of the starting substrate **9** by $\Delta\delta$ = 3.0 and 1.5 ppm, respectively. However, the main difference between the ^{13}C NMR spectra of the starting 2,2-DM-1,3-DAP and product **10** was the appearance of a downfield signal with δ = 166.0 characteristic of the carbon atom of the carboxylate anion. These differences in spectral characteristics indicate the transformation of the starting substrate **9** during electrolysis.

To further determine the structure of the new compound **10**, a set of its 2D spectra was recorded: {^1H—^{13}C} HSQC (heteronuclear single-quantum correlation spectroscopy) (Fig. 8, *a*) and {^1H—^{13}C}HMBC (heteronuclear multiple-bond correlation spectroscopy) (Fig. 8, *b*), {^1H—^1H}gCOSY (proton multiple-bonds correlation spectroscopy) (Fig. 8, *c*) and {^1H—^1H}gNOESY (nuclear Overhauser effect spectroscopy) (Fig. 8, *d*) in a D_2O solution at 298 K.

In the {^1H—^{13}C}HSQC NMR spectrum of compound **10**, for the carbon atom with a chemical shift δ = 47.3, a cross-peak is observed only with CH_2 protons, which have a chemical shift δ = 2.62, while for the carbon atom with a shift δ = 48.8, a cross-peak is observed only with CH_2 protons having a chemical shift δ = 2.80 (see Fig. 8, *a*). In the {^1H—^{13}C}HMBC NMR spectrum of compound **10**, for the carbon atom with a chemical shift δ = 166.0,

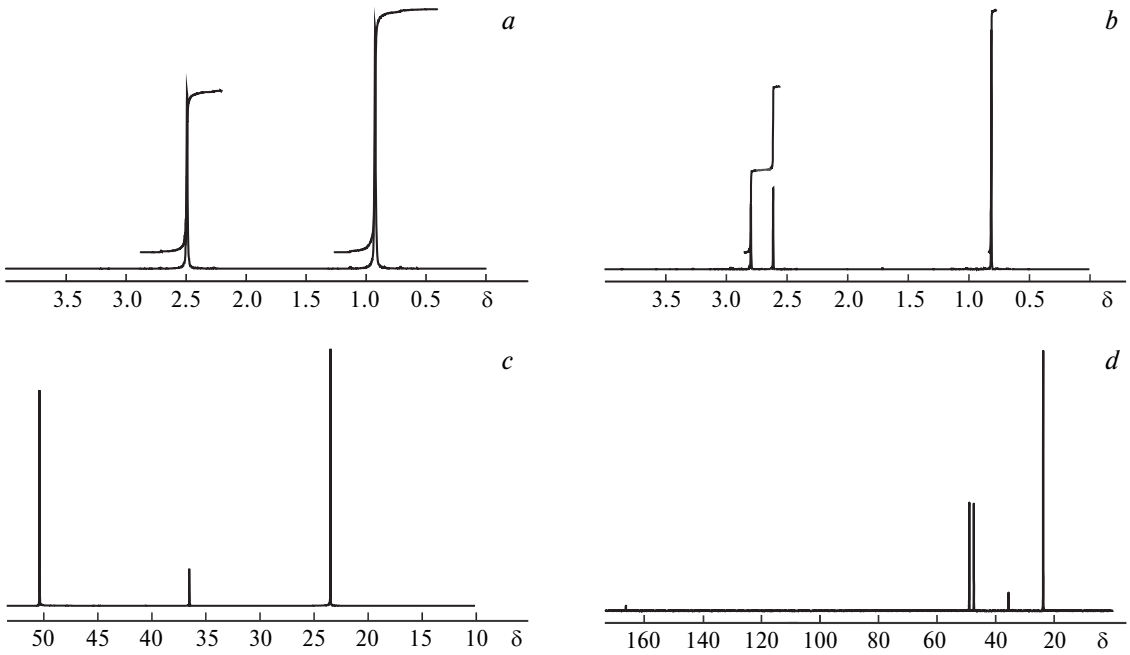

Fig. 7. Fragments of ^{1}H (*a*, *b*) and ^{13}C NMR spectra (*c*, *d*) of diaminoalkane **9** (*a*, *c*) and compound **10** (*b*, *d*) in D_2O.

a cross-peak is observed only with CH_2 protons (δ = 2.80) (see Fig. 8, *b*), which confirms the chemical nonequivalence of the carbon atoms of CH_2 groups belonging to the same molecule **10**.

The 2D homonuclear spectrum {$^{1}H—^{1}H$}gCOSY shows how far from each other the protons are within the molecule, namely, are they separated by one or two—four bonds. In the 2D {$^{1}H—^{1}H$}gNOESY NMR spectrum (nuclear Overhauser effect), which shows the spatial arrangement of protons in a molecule relative to each other, cross-peaks are observed between the protons of different CH_2 groups of a single molecule **10**, which is possible only when it has a nonlinear structure (see Fig. 8, *d*).

According to the results of elemental analysis, IR and NMR spectroscopy, it is likely that the new compound is an internal salt of carbamic acid (3-ammonio-2,2-dimethylpropyl carbamate) with the molecular formula $C_6H_{14}N_2O_2$. X-ray diffraction results confirmed the proposed structure of compound **10**, shown in Fig. 9. The hydrogen atoms of the ammonium group form intermolecular hydrogen bonds with the oxygen atoms of three other molecules (Table 3), developing a three-dimensional network of hydrogen bonds; the carbamate group hydrogen atoms are not involved in the formation of hydrogen bonds.

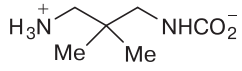

10

In the work,[24] compound **10** (3-ammonio-2,2-dimethylpropyl carbamate) was synthesized as a dihydrate, obtained by maintaining a solution of diamine **9** in a small amount of diluted acetic acid in air for a long period of time (a day); its structure was confirmed by IR/Raman spectra and X-ray diffraction results.[24] In contrast to the structure of product **10** which we determined, the structure of the **10** • $2H_2O$ solvatomorph (CCDC number — 1844554, Cambridge Crystallographic Data Center code — TIXROK) contains intra- and intermolecular hydrogen bonds. The formation of these bonds involves the hydrogen atoms of both ammonium and carbamate groups, as well as all the hydrogen atoms of water molecules. The

Table 3. Parameters of intermolecular hydrogen bonds in a crystal of compound **10** (D is donor, A is acceptor)

D—H...A bonds	d/Å			DHA angle/deg	Symmetry operation
	D—H	H...A	D...A		
N(2)—H(2C)...O(1^{i})	0.94(2)	1.80(3)	2.7333(18)	173(2)	$-x, y + 1/2, -z + 1/2$
N(2)—H(2D)...O(2^{ii})	0.88(2)	1.88(2)	2.7589(18)	178(2)	$-x + 1/2, -y + 1, z - 1/2$
N(2)—H(2E)...O(2^{iii})	0.89(3)	1.90(3)	2.7807(19)	166(2)	$-x + 1, y + 1/2, -z + 1/2$

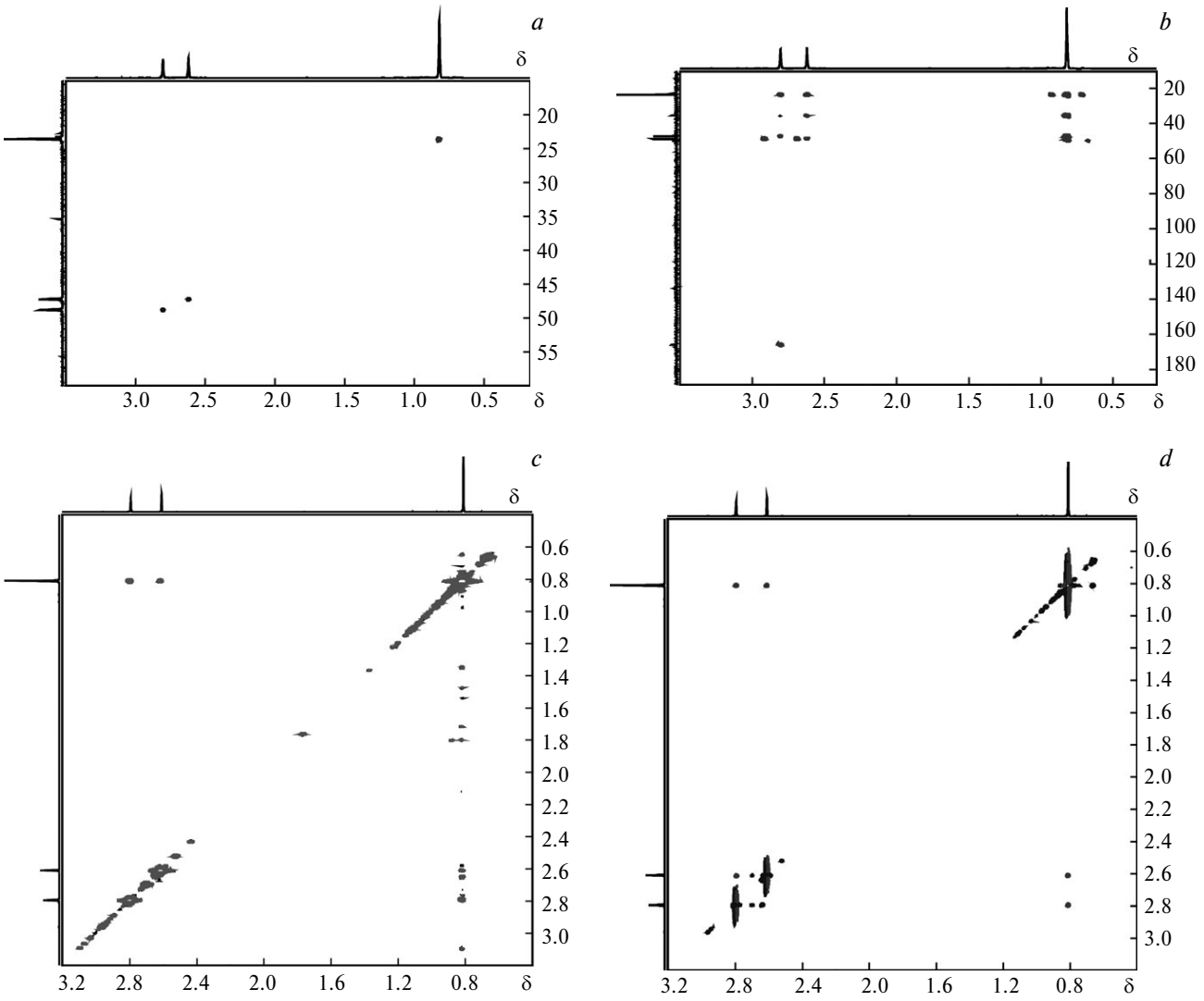

Fig. 8. 2D spectra {^{1}H—^{13}C}HSQC (*a*), {^{1}H—^{13}C}HMBC (*b*), {^{1}H—^{1}H}gCOSY (*c*), and {^{1}H—^{1}H}gNOESY (*d*) of new compound **10** (D_2O + TSP).

other bond lengths in these structures are similar. No NMR spectra of dihydrate **10** • $2H_2O$ were recorded. The authors believe that compound **10** was formed as a result of the interaction of the starting amine with carbon dioxide CO_2 in air. Clearly, in our case, compound **10** was formed in a similar way upon contact of the free ligand with CO_2 during electrolysis, which lasted for 50 h. The presence of free diamine in the solution is probably a result of insufficient stability of its complex with gold, which, apparently, quite rapidly reduces at the cathode, or decomposes in the solution with the formation of colloidal gold. The insufficient stability of the 2,2-DM-1,3-DAP **9** complex with gold is probably a result of steric hindrances due to the two methyl groups bound to the C(2) carbon atom of this ligand.

The formation of salts of carbamic acid **11** during the transmission of a CO_2 current through a solution of the corresponding amine is a fairly well-known process.[26,27] However, it is usually carried out using monoalkylamines and, therefore, the formation of type **10** internal salt is very rare (Scheme 1).

Scheme 1

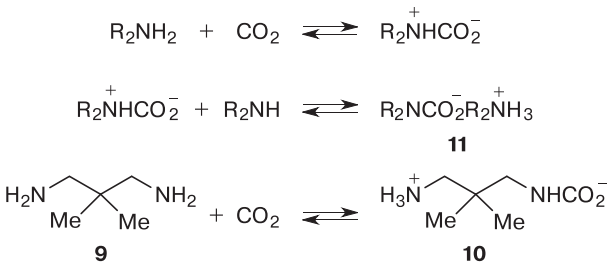

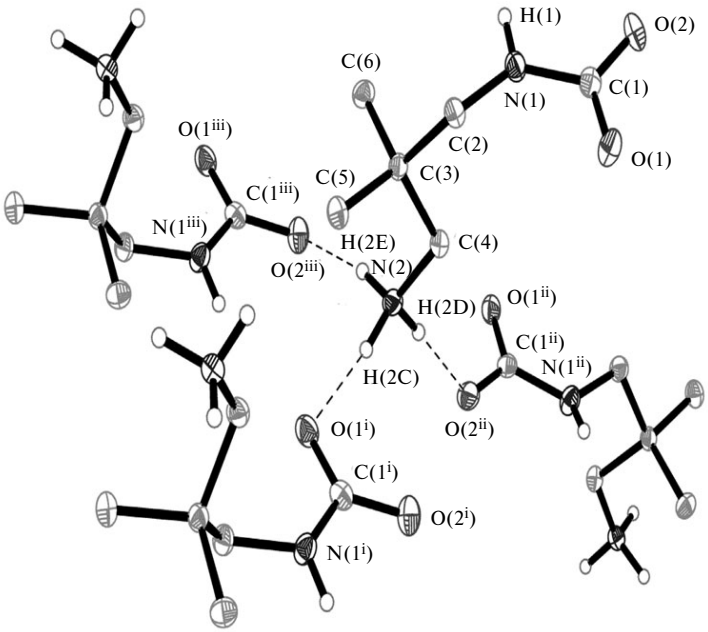

Fig. 9. Geometry and hydrogen bonds of compound **10**; hydrogen atoms of methyl and methylene groups are not shown. Anisotropic thermal vibrations of hydrogen-free nitrogen atoms are given with a 50% probability (for symmetry operations see Table 3).

In conclusion, the study of the corrosion of an Au anode by gravimetry and cyclic voltammetry in a weakly basic aqueous solution of substrate **9** showed that the products of anode corrosion (gold complexes with 2,2-DM-1,3-DAP) under galvanostatic conditions reduce on the steel cathode with the formation of an electrolytic precipitate of crystalline Au on the cathode and the formation of colloidal gold nanoparticles in the electrolyte medium. Isolated from the reaction solution after the separation of colloidal gold, product **10**, obtained upon contact of the free ligand with atmospheric CO_2 during electrolysis, is the internal salt of carbamic acid (3-ammonio-2,2-dimethylpropylcarbamate).

The authors are grateful to the Department of Structural Research of the N. D. Zelinsky Institute of Organic Chemistry of the Russian Academy of Sciences for carrying out electron microscopy of the samples.

This work was financially supported of the Science Schools Development Program of the N. D. Zelinsky Institute of Organic Chemistry of the Russian Academy of Sciences.

The authors declare no competing interest.

References

1. X. M. Zhang, G. Senanayake, *Miner. Process. Extr. Metall. Rev.*, 2016, **37**, 385.
2. S. S. Konyratbekova, A. Baikonurova, A. Akcil, *Miner. Process. Extr. Metall. Rev.*, 2015, **36**, 198.
3. X. Yang, M. S. Moats, J. D. Mille, *Electrochim. Acta*, 2010, **55**, 3643.
4. S. Ye, C. Ishibashi, K. Shimazu, K. Uosaki, *J. Electrochem. Soc.*, 1998, **145**, 1614.
5. M. Tian, W. G. Pell, B. E. Conway, *J. Electroanal. Chem.*, 2003, **552**, 279.
6. M. Tian, W. G. Pell, B. E. Conway, *Corros. Sci.*, 2008, **50**, 2682.
7. S. R. Smith, E. Guerra, S. Siemann, J. L. Shepherd, *Electrochim. Acta*, 2011, **56**, 8291.
8. A. P. Simakova, M. D. Vedenyapina, V. V. Kuznetsov, N. N. Makhova, A. A. Vedenyapin, *Russ. J. Phys. Chem. A*, 2014, **88**, 331.
9. M. D. Vedenyapina, V. V. Kuznetsov, N. N. Makhova, A. A. Vedenyapin, *Russ. J. Phys. Chem. A*, 2016, **90**, 1903.
10. M. D. Vedenyapina, G. Ts. Ubushieva, V. V. Kuznetsov, N. N. Makhova, A. A. Vedenyapin, *Russ. J. Phys. Chem. A*, 2016, **90**, 2312.
11. M. D. Vedenyapina, V. V. Kuznetsov, D. I. Rodikova, N. N. Makhova, A. A. Vedenyapin, *Mendeleev Commun.*, 2018, **28**, 181.
12. M. D. Vedenyapina, V. V. Kuznetsov, N. N. Makhova, D. I. Rodikova, *Russ. J. Phys. Chem. A,* 2019, **93**, 466.
13. M. D. Vedenyapina, V. V. Kuznetsov, N. N. Makhova, D. I. Rodikova, *Russ. Chem. Bull.*, 2019, **68**, 1997.
14. M. D. Vedenyapina, V. V. Kuznetsov, N. N. Makhova, D. I. Rodikova, *Russ. Chem. Bull.*, 2020, **69**, 1884.
15. V. V. Kachala, L. L. Khemchyan, A. S. Kashin, N. V. Orlov, A. A. Grachev, S. S. Zalesskiy, V. P. Ananikov, *Russ. Chem. Rev,* 2013, **82**, 648.
16. *Bruker. APEX-III*, Bruker AXS Inc., Madison (WI), USA, 2019.
17. L. Krause, R. Herbst-Irmer, G. M. Sheldrick, D. Stalke, *J. Appl. Cryst.*, 2015, **48**, 3; DOI: 10.1107/S1600576714022985.

18. G. M. Sheldrick, *Acta Crysttallogr.*, *Sect. A: Found. Crysttallogr.*, 2015, **A71**, 3; DOI: 10.1107/S2053273314026370.
19. G. M. Sheldrick, *Acta Crysttallogr.*, *Sect. C*, 2015, **C71**, 3; DOI: 10.1107/S2053229614024218.
20. E. Laviron, *J. Electroanal. Chem*., 1979, **101**, 19.
21. L. A. Dykman, N. G. Khlebtsov, *Russ. Chem. Rev.*, 2019, **88**, 229.
22. A. A. Revina, K. F. Chernyshova. N. Yu. Tabachkova, Yu. N. Parhomenko, *Russ. Chem. Bull.*, 2019, **68**, 1164.
23. R. T. Conley, *Infrared Spectroscopy*, Allyn and Bacon, Boston, 1966.
24. A. Finch, P. N. Gates, R. Radcliffe, F. N. Dicson, F. F. Bentley, *Chemical Applications of Far Infrared Spectroscopy*, Academic Press, New York, London, 1970.
25. J. Heimgert, D. Neumann, G. J. Reis, *Molbank,* 2018, M1015; DOI: 10.3390/M1015.
26. R. N. Salvatore, S. I. Shin, A. S. Nagle, K. W. Jung, *J. Org. Chem.,* 2001, **66**, 1035.
27. G. Sartori, D. W. Savage, *Ind. Eng. Chem. Fundam*, 1983, **22**, 239.

Received November 9, 2020;
in revised form December 17, 2020;
accepted December 22, 2020